

Title	Impact Property at Cryogenic Temperature of Candidate Materials for Fusion Reactor and Their Electron Beam Welded Joints(Materials, Metallurgy & Weldability)
Author(s)	Kaga, Seiichi; Fukuhara, Isamu; Fujii, Katsuhiro et al.
Citation	Transactions of JWRI. 1991, 20(2), p. 231-240
Version Type	VoR
URL	<a href="https://doi.org/10.18910/3903">https://doi.org/10.18910/3903</a>
rights	
Note	

***Osaka University Knowledge Archive : OUKA***

<https://ir.library.osaka-u.ac.jp/>

Osaka University

# Impact Property at Cryogenic Temperature of Candidate Materials for Fusion Reactor and Their Electron Beam Welded Joints

Seiichi KAGA\*, Isamu FUKUHARA\*\*, Katsuhiko Fujii\*\*\*, Kouichi OGAWA\*\*\*\*, Yoshiaki YAMAMOTO\*\*\*\*\*, Nobuyuki ABE\*\*\*\*\* and Michio TOMIE\*\*\*\*\*

## Abstract

Impact properties at cryogenic temperature of candidate materials for fusion reactor and their electron beam welded joints are investigated by using instrumented Charpy impact testing apparatus. Materials used are aluminum alloys (A7N01, A5083, A6061), JFMS (Japanese Ferritic Martensitic Steel) and two kinds of high manganese steel. Although JFMS is a steel for high temperature use, the impact test is conducted at same cryogenic temperature as the cases of the other materials.

Testing results are obtained as follows.

1. Base metal and welded joint of aluminum alloys exhibit high absorbed energy at low temperature.
2. Base metal and welded joint of JFMS show an absorbed energy transition temperature at near a room temperature.
3. Base metal and welded joint of high manganese steel, A-T(18Mn), exhibit an abrupt decreasing of absorbed energy at 77K, but base metal and welded joint of high manganese steel, B-T(22Mn-0.2N), exhibit gradual increasing of maximum strength and decreasing of ductility with decreasing of test temperature.

**KEY WORDS :** (Fusion Reactor Material) (Instrumented Charpy Impact Test) (Aluminum Alloy) (Ferritic Martensitic Steel) (High Manganese Steel)

## 1. Introduction

Aluminum alloys, ferritic martensitic steel and high manganese steels are selected as testing materials in this study. Aluminum alloys are expected as structural materials at cryogenic temperature<sup>1)</sup>, because they do not exhibit low temperature brittleness and are excellent in processing ability, weldability, and decrement characteristic of induction radioactivity. As a ferritic martensitic steel, JFMS (Japanese Ferritic and Martensitic Steel) is used in this experiment. Property at high temperature of JFMS has been clarified gradually<sup>2)</sup>, However, there is insufficient data on its welded joint. Though JFMS is a steel for high temperature use, the impact test is conducted at same cryogenic temperature as the cases of the other materials. For purpose of economical steels, high manganese steel is made by replacing Ni by Mn in Nickel-Chromium austenite. In recent years, it has been studied as a nonmagnetic material at cryogenic temperature, and has been also investigated to use as main structural steel of

experimental nuclear fusion reactor and so on<sup>3),4)</sup>.

Toughness of various materials can be easily evaluated by Charpy impact test. In particular, the information of absorbed energy and maximum load of materials can be obtained by using an instrumented Charpy impact testing apparatus. The information which can be obtained from Charpy impact test have a very important significance in order to make clear the fracture mechanism of various materials in the case of impact as well as tension test.

Thus, the purpose of this study is to investigate toughness of materials when aluminum alloys, JFMS, high manganese steels and their electron beam welded joints are used at cryogenic temperature.

## 2. Experimental Method

### 2.1 Testing materials

Chemical compositions are shown in **Table 1**. Materials used are aluminum alloys (A7N01, A5083, A6061),

† Received on Nov 9, 1991

\* Professr, Osaka Institute of Technology

\*\* Resarch Assistant, University of Osaka Pref.

\*\*\* Resarch Assistant, Osaka Institute of Technology

\*\*\*\* Associate Professor, University of Osaka Pref.

\*\*\*\*\* Associate Professor, Setsunan University

\*\*\*\*\* Associate Professor

Transactions of JWRI is published by Welding Research Institute, Osaka University, Ibaraki, Osaka 567, Japan

Table 1 Chemical compositions of materials used.

Materials	Chemical compositions (wt%)																	
	Al	Cu	Mg	Zn	Ti	Zr	Fe	Mn	Cr	Si	C	P	S	Ni	Mo	V	Nb	N
A7N01-T6	BAL.	0.16	1.12	4.73	0.01	0.15	0.11	0.30	0.06	0.05	-	-	-	-	-	-	-	-
A5083-0	BAL.	0.01	4.61	0.03	0.01	-	0.11	0.68	0.13	0.05	-	-	-	-	-	-	-	-
A6061-T6	BAL.	0.18	0.50	0.04	0.005	-	0.12	0.01	0.00	0.72	-	-	-	-	-	-	-	-
JFMS	-	-	-	-	-	-	BAL.	0.58	9.85	0.67	0.05	0.009	0.006	0.94	2.31	0.12	0.06	-
A-T	-	-	-	-	-	-	BAL.	17.0	6.5	4.5	0.03	0.02	0.02	-	-	-	-	-
B-T	-	-	-	-	-	-	BAL.	22.0	6.5	4.5	0.03	0.02	0.02	-	-	-	-	0.2

JFMS, and two kinds of high manganese steels which are called as A-T and B-T. Each aluminum alloy is materials of hot rolling and 15 mm thick. JFMS is hot rolling steel and has a thickness of 12 mm. After JFMS at 1223K was cooled in air, it was annealed at 1073K. High manganese steel is 13mm thick. After it was forged at 1273 ~ 1473K, it was treated with water toughening for one hour at 1373K.

## 2.2 Electron beam welding conditions and processing of the materials

Figure 1 shows a schematic diagram of flat and horizontal position electron beam welding method. When horizontal position welding was performed, a vertical electron beam was deflected in 90° to be horizontal beam by a beam deflector. JFMS steel was welded at horizontal position with beam oscillation and other materials were welded at flat position without oscillation. Welding conditions are shown in Table 2.

Size of the specimen is shown in Fig. 2. Small size of specimen is used under the consideration of evaporation of helium and capacity of neutron irradiation apparatus which will be used after this experiment.

Sampling of specimen for instrumented Charpy impact test from welded joint is illustrated in Fig. 3. Specimens are notched in the direction parallel or perpendicular to plate in order to examine an anisotropy of materials. These are called as type T or type S. Type T is made of only base metal of A5083. Notch part is sampled to be just the center of weld metal. The same specimens as weld metal are obtained from base metal which is independent of heat.

## 2.3 Experimental apparatus

The information of crack initiation energy, crack propagation energy, yield load and maximum load can be obtained by using an instrumented Charpy impact testing apparatus. Moreover, it can be made more practical application to estimate toughness of the materials than usual Charpy impact testing apparatus.

Block diagram and apparatus for instrumented Charpy impact test are shown in Fig. 4. Each apparatus is set in order of block diagram shown in Fig. 4, load-time curves of various test specimens are recorded on an

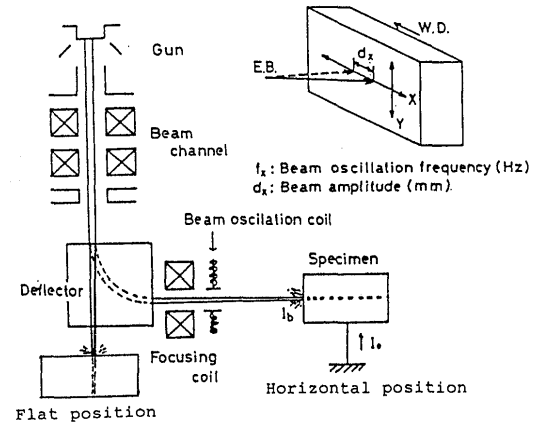


Fig. 1 Schematic diagram of flat and horizontal position welding method.

Table 2 Welding conditions of materials used.

Materials	Welding position	Beam voltage (kV)	Beam current (mA)	Welding speed (m/min)
A7N01-T6	Flat	60	80	0.6
A5083-0	Flat	60	80	0.6
A6061-T6	Flat	60	90	0.3
JFMS*	Horizontal	100	60	0.6
A-T	Flat	60	80	0.3
B-T	Flat	60	80	0.3

\*Beam oscillation:  $f_x=30(\text{Hz})$ ,  $d_x=3(\text{mm})$  (Vacuum  $6.7 \times 10^{-2} \text{Pa}$ )

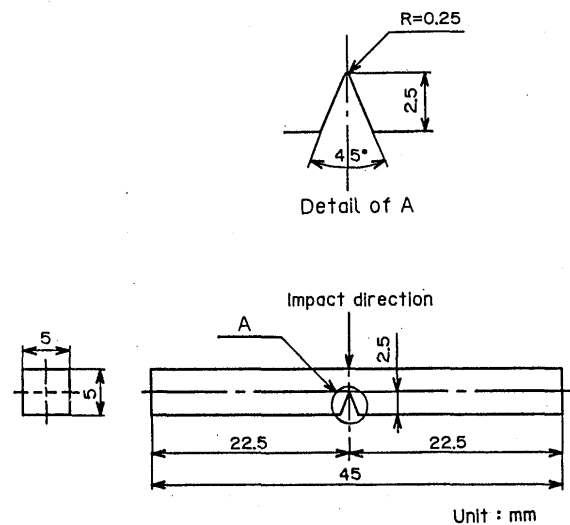


Fig. 2 Specimen for instrumented Charpy impact test.

electromagnetic oscillograph.

Examples of relation between total absorbed energy ( $E_t$ ) and energy by dial reading ( $E_r$ ) are shown in Fig. 5.  $E_t$  is obtained from area of load-displacement curve,  $E_r$  is calculated according to JIS Z 2242 from dial difference before and after impact test. As shown in Fig. 5, values of  $E_t$  and  $E_r$  are not necessarily the same. Thus, the cause of differences between  $E_t$  and  $E_r$  in this experiment is considered to be energy loss due to longitudinal vibration by a hammer and vibration by a repulsion of specimen and hammer in the initial impact<sup>5)</sup>. Then, only  $E_r$  is used to consider the experimental results of this study.

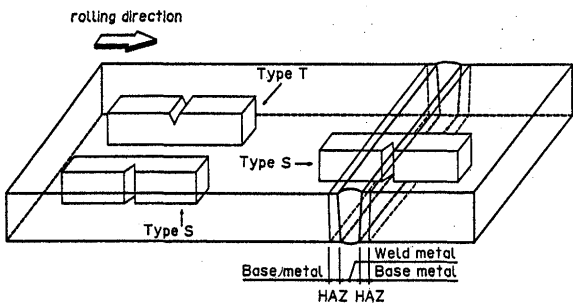


Fig. 3 Sampling of specimen for instrumented Charpy impact test.

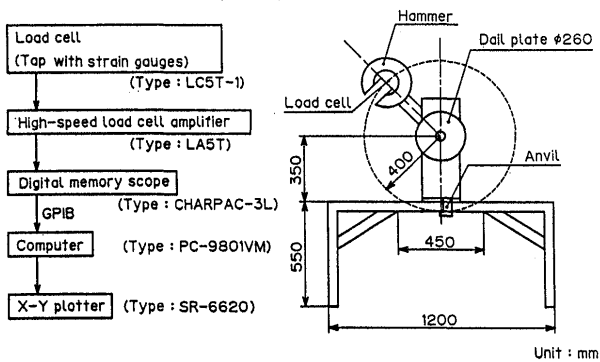


Fig. 4 Block diagram and apparatus for instrumented Charpy impact test.

A method of keeping a specimen at temperature below 77K is not defined in the items of JIS. After a specimen is cooled by liquid nitrogen, it is set on an anvil quickly and is put to the impact test. Time required for a cooling specimen to set on the anvil is about 5 seconds, temperature of specimen raises to approximately 8K at the regular intervals. A method<sup>6)</sup> developed by National Research Institute for Metals is referred to cool and keep a specimen at cryogenic temperature.

Experimental apparatus for cryogenic instrumented Charpy impact test is shown in Fig. 6. In this apparatus a specimen is put in a capsule of polystyrene foam. While liquid helium flows through a transfer tube, a specimen covered with a capsule is put to the impact test. As a result of this method, a specimen can be kept at a temperature in the region of 4K. Therefore, it has been reported that there is almost no energy absorbed by a capsule, because a portion of polystyrene foam which is touched by a hammer is thinned to lessen energy absorbed by a hammer. Then, it was confirmed in the impact test used an only capsule that total absorbed energy is very low and nearly zero. Results of measuring specimen temperature of A7NO1 and JFMS in the case when the temperature is reduced to about 4K are shown in Fig. 7. In order to measure a specimen temperature, thermocouple is used and is put in the middle of the hole drilled in the opposite side of notched part of a specimen. As seen in Fig. 7, a specimen temperature reaches nearly 4K in about 90 seconds after a specimen is started to cool. This impact test consumes about 0.6 liter of liquid helium per specimen.

2.4 Experimental conditions

Testing temperature are room temperature (293K), ethyl alcohol + liquid nitrogen temperature (173K), liquid nitrogen temperature (77K) and liquid helium temperature (4.2K). In impact test at liquid helium temperature, only base metal is conducted. Capacity of testing machine is 29.4J, impacting velocity of a hammer

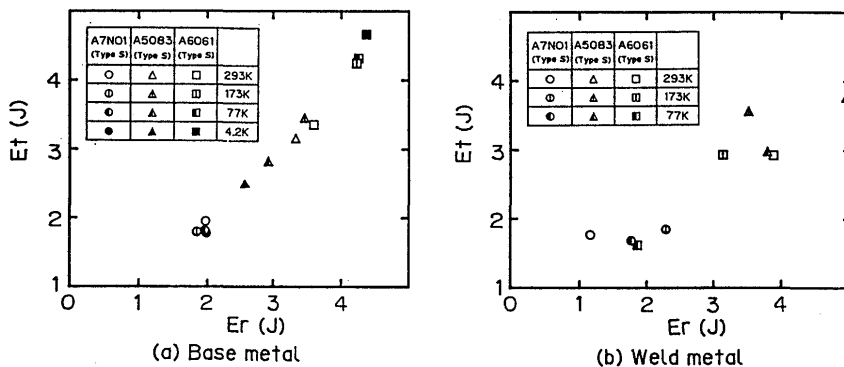


Fig. 5 Relation between total absorbed energy ( $E_t$ ) and energy by dial reading ( $E_r$ ) of Al alloys at various test temperatures.

is 3.69m/sec. There is a width of 30mm between anvils. Load-time curves recorded by an electromagnetic oscillograph are processed by computer to transform into the load-displacement curves

### 3. Results and Consideration

#### 3.1 Load-displacement curve

Load-displacement curves of various specimens obtained by this experiment are shown in Fig. 8 ~ Fig. 13 respectively. It can be seen from Figs. 8 ~ 10 in each specimen of aluminum alloys that maximum load increases with decreasing of test temperature. Characteristic change of load against displacement can be observed in type T of base metal at 77K and 4.2K as

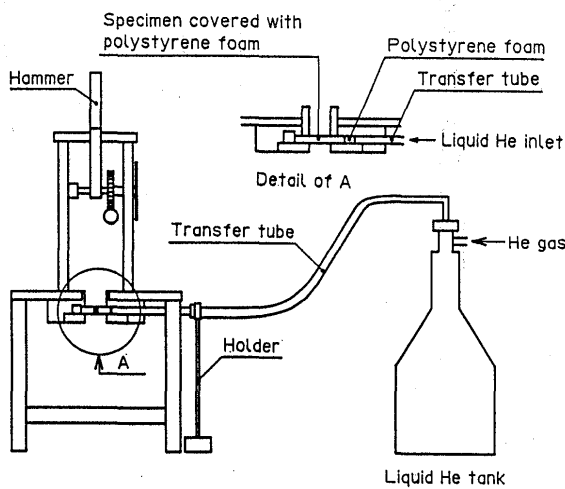


Fig. 6 Apparatus for cryogenic instrumented Charpy impact test.

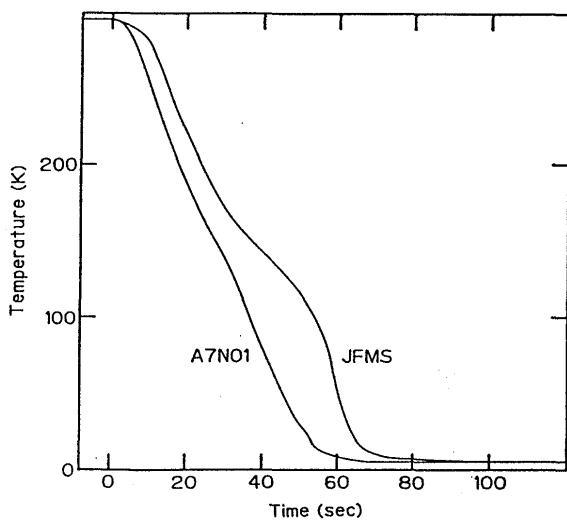


Fig. 7 Change in specimen temperatures of A7N01 and JFMS covered with polystyrene foam against cooling time.

shown in Fig. 9. In type S of base metal, however, characteristic change can not be observed. It can be considered that this special change of load is due to formation and propagation of lamellar flaking caused by rolling structure. Then, Fig. 14 shows these appearances of lamellar flaking.

As it is generally considered that lamellar flaking is related to maximum load, total absorbed energy and test temperature, it is rational to estimate that lamellar flaking is caused by inclusion grains which crystallizes or precipitates grain boundary. In this study, structure

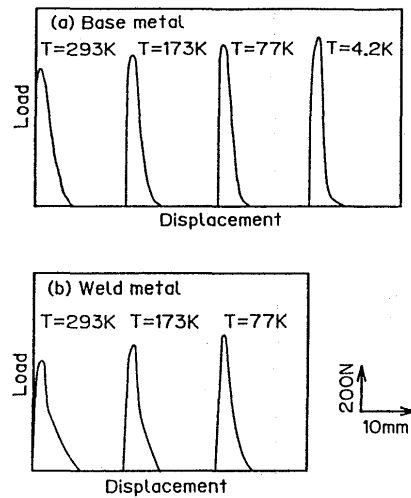


Fig. 8 Load-displacement curves of A7N01 at various test temperatures.

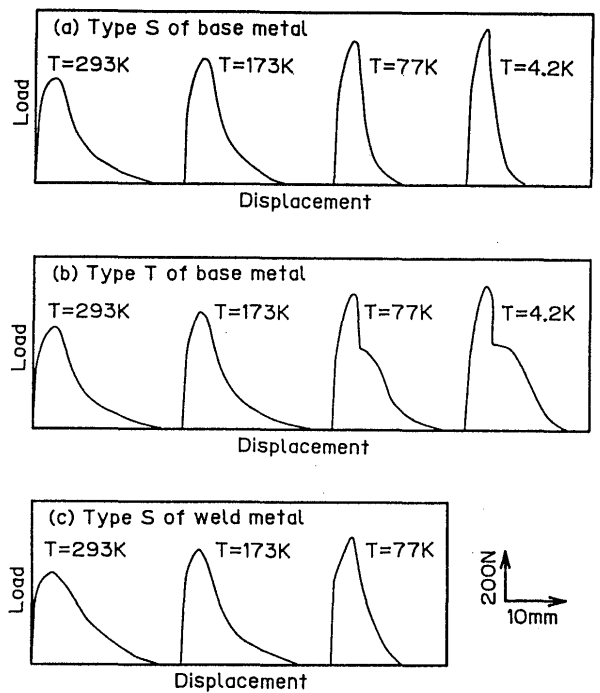
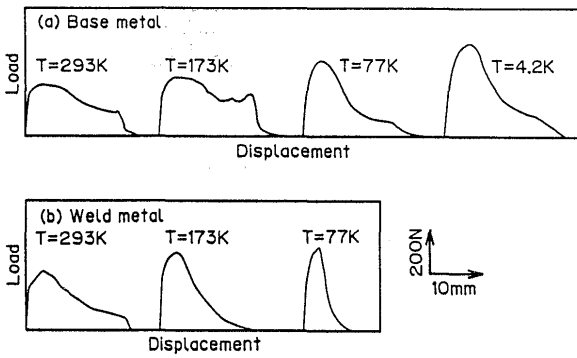


Fig. 9 Load-displacement curves of A5083 at various test temperatures.



Load-displacement curves of A6061 at various test temperatures

Fig. 10 Load-displacement curves of A6061 at various test temperatures.

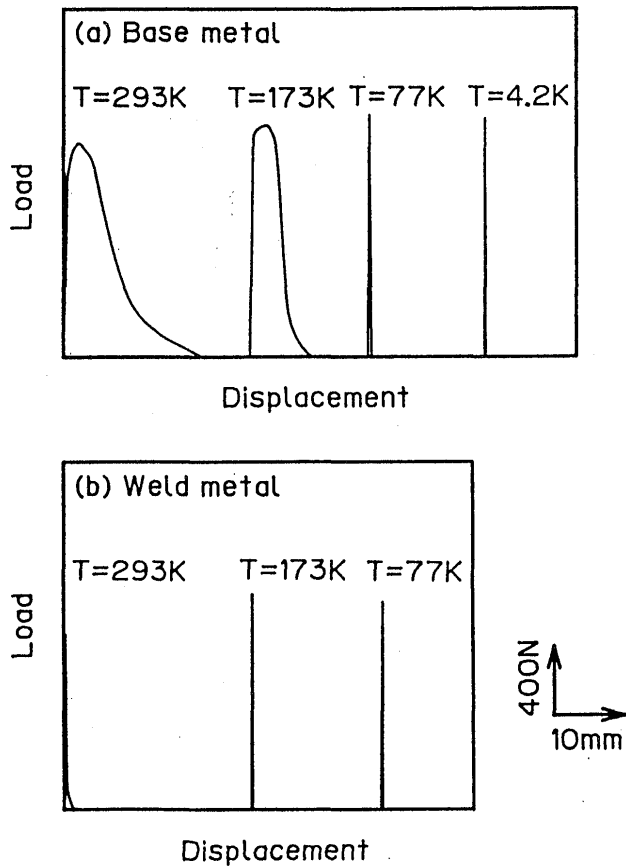


Fig. 11 Load-displacement curves of JFMS at various test temperatures.

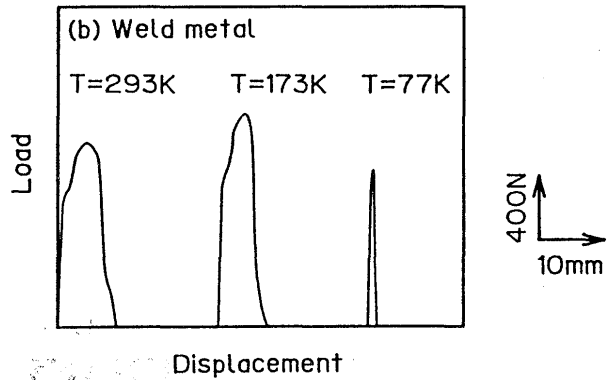
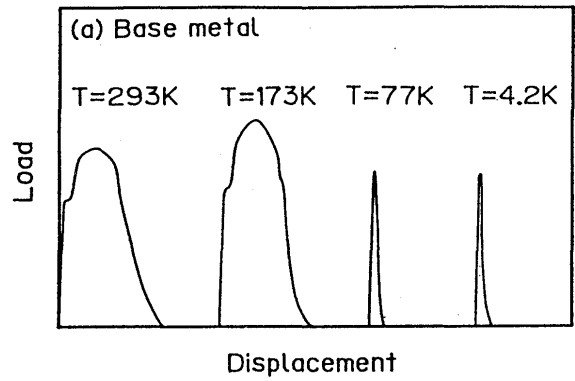


Fig. 12 Load-displacement curves of A-T at various test temperatures.

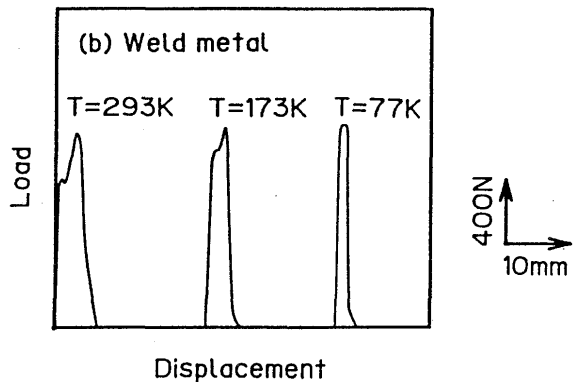
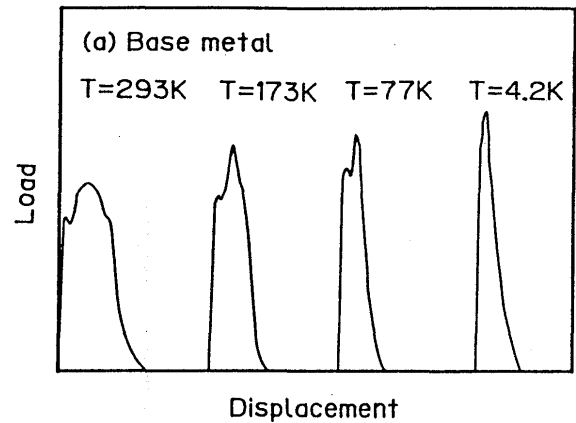


Fig. 13 Load-displacement curves of B-T at various test temperatures.

arranged along a rolling direction or grains of intermetallic compound corresponded to second phase seem to exist as  $\beta$  phase ( $Al_2Mg_2$ ) or  $Mg_2Si$ , that is lamellar flaking is due to segregate  $\beta$  phase or Mg from the grain boundary<sup>7),8)</sup>, it is considered that lamellar flaking arises when these precipitated grains which expand by rolling cause low temperature brittleness<sup>9)</sup>.

From Fig. 11 it is seen that obvious brittleness is observed in JFMS base metal at 77K, and weld metal shows brittleness already at room temperature.

It is found from Figs. 12 and 13 that total absorbed energy of A-T base and weld metals at temperature below 77K is very low and B-T is not low as compared to A-T.

**3.2 Effect of test temperature on energy**

Dependence of test temperature on energy of various specimens and their electron beam welded joints is shown in Figs. 15 ~ 20. Then, the general definition of  $E_t$ ,  $E_i$  and  $E_p$  is shown in Fig. 21. Absorbed energy until load reaches the maximum is represented as crack initiation energy,  $E_i$ , absorbed energy from the maximum load to fracture is expressed as crack propagation energy,  $E_p$ ,

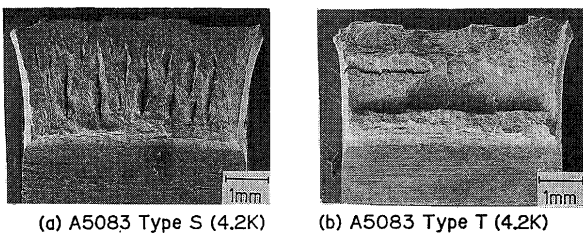


Fig. 14 Microphotographs of laminated fracture surface of A5083 base metal.

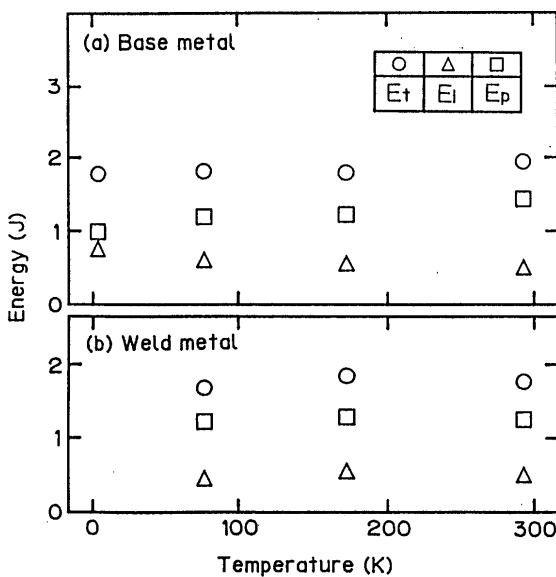


Fig. 15 Change in total absorbed energy ( $E_t$ ), crack initiation energy ( $E_i$ ) and crack propagation energy ( $E_p$ ) of A7N01 at various test temperatures.

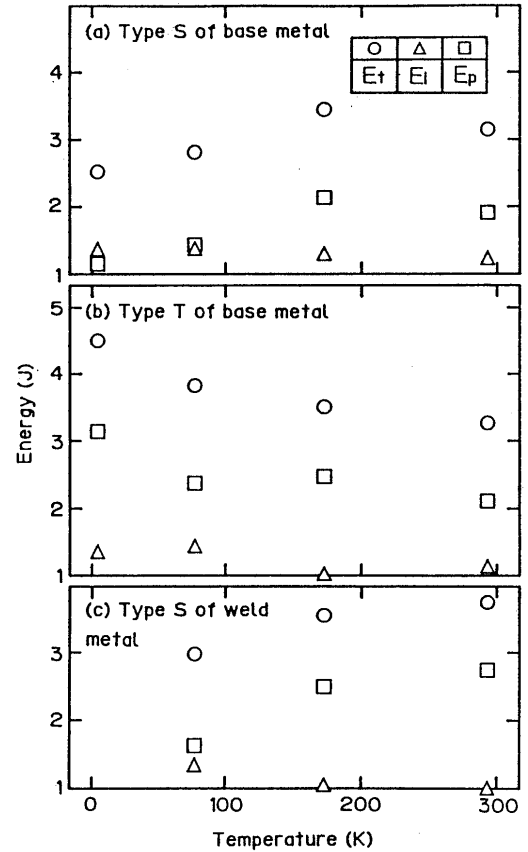


Fig. 16 Change in total absorbed energy ( $E_t$ ), crack initiation energy ( $E_i$ ) and crack propagation energy ( $E_p$ ) of A5083 at various test temperatures.

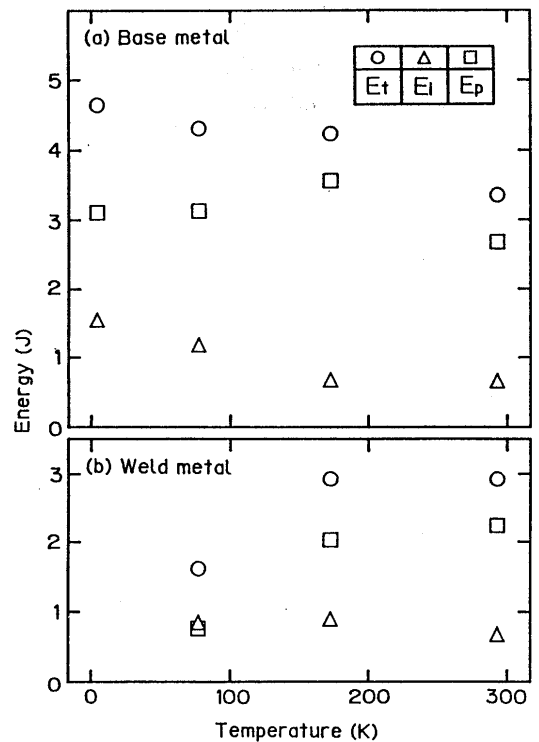


Fig. 17 Change in total absorbed energy ( $E_t$ ), crack initiation energy ( $E_i$ ) and crack propagation energy ( $E_p$ ) of A6061 at various test temperatures.

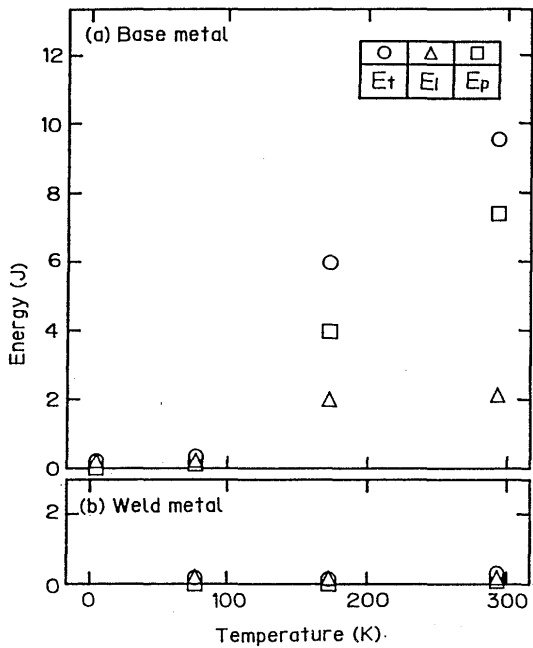


Fig. 18 Change in total absorbed energy ( $E_t$ ), crack initiation energy ( $E_i$ ) and crack propagation energy ( $E_p$ ) of JFMS at various test temperatures.

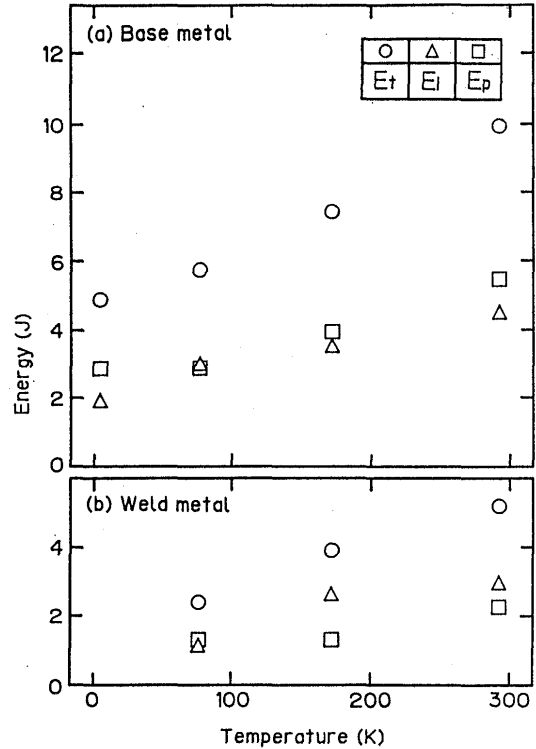


Fig. 20 Change in total absorbed energy ( $E_t$ ), crack initiation energy ( $E_i$ ) and crack propagation energy ( $E_p$ ) of B-T at various test temperatures.

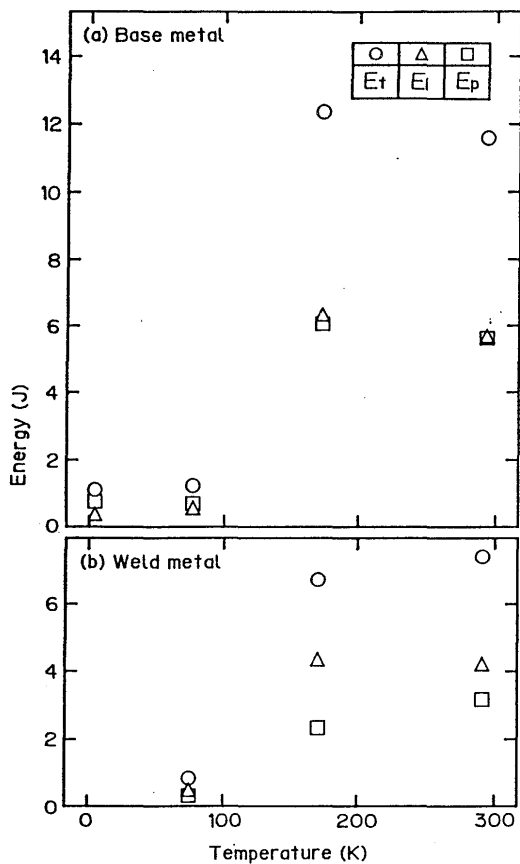


Fig. 19 Change in total absorbed energy ( $E_t$ ), crack initiation energy ( $E_i$ ) and crack propagation energy ( $E_p$ ) of A-T at various test temperatures.

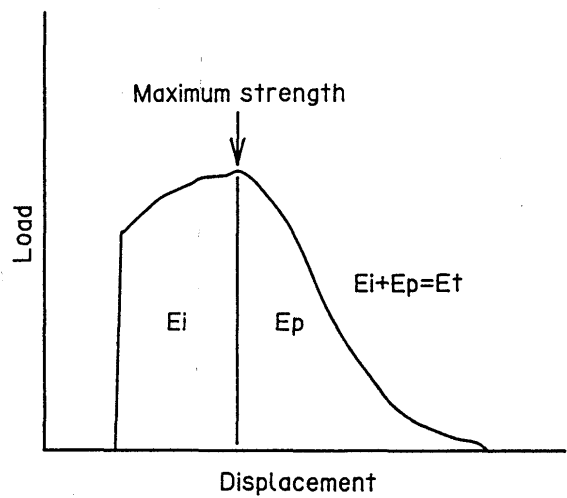


Fig. 21 Schematic figure of load-displacement curve.

total absorbed energy,  $E_t$ , can be denoted as  $E_t = E_i + E_p$ .

From Fig. 15 it is found that the crack initiation energy increases with decreasing of test temperature in A7NO1 base metal. Crack propagation energy has a decreasing tendency, thus total absorbed energy does not change with decreasing of test temperature. As for welded joints, these values do not vary. From the fact as described above, it is evident that A7NO1 base metal and weld metal maintain about equal toughness at room



temperature to the extent of low temperature.

In Fig. 16 it is seen that total absorbed energy of A5083 base metal and weld metal decreases with decreasing of test temperature. Crack initiation energy does not change much, crack propagation energy decreases. From these results of A5083, generating process of crack is not affected very much by low temperature, and propagating rate of crack is accelerated with decreasing of temperature. Therefore, decrease of total absorbed energy, as it is called, lowering of toughness is observed. This change with temperature is not a ductility - brittle transition, each temperature shows the upper shelf in fracture energy. Energy of type S base metal at 4.2K shows a decrease of about 0.6J as compared to 293K. In the same comparison as described above, energy of weld metal shows a drop of about 0.7J. It is necessary to consider these facts in the case of using as a structural material for vessel of low temperature. It is thought that this decrease is caused by 0.2% proof stress which becomes higher<sup>10)</sup>.

Total absorbed energy of type T of A5083 base metal has a tendency to increase with decreasing of temperature. Crack initiation energy at 77K and 4.2K increases only slightly in comparison with 293K, crack propagation energy increases with decreasing of temperature.

Increase and decrease of crack propagation energy that depends on a difference of these type are affected by the crack direction which crosses or passes through lamellar structure. In other words, increase of crack propagation energy of type T is considered as a result of lamellar flaking which is generated to cross a lamellar structure by crack.

It is seen from Fig. 17 that total absorbed energy of A6061 base metal increases with decreasing of temperature. And, when temperature goes down, crack initiation energy increases and crack propagation energy increases slightly.

In these aluminum alloys, with respect to toughness that depends on change of temperature, A6061 is the most excellent among base metals, A5083 is the most excellent in weld metals. As a whole, A5083 shows the most splendid toughness.

Next, results of JFMS base metal are indicated in Fig. 18, Et, Ei and Ep decrease with decreasing of temperature. Energy at 77K is close to 0J, thus, it is found that it has become brittle. From this figure, it is seen that transition temperature is around 135K. It is considered that weld metal has already become brittle at 293K, transition temperature is above room temperature. And, from the fact mentioned above, it is obvious that PWHT is required for weld metal.

As shown in Fig. 19, absorbed energy of both base and

weld metals of A-T decreases abruptly at 77K, crack initiation energy and crack propagation energy show a similar tendency. It is considered that this is caused by strain induced martensite generated by impact test at cryogenic temperature. As this strain induced martensite is generated<sup>11)</sup> and contains  $\alpha'$  martensite of bcc and  $\epsilon$  martensite of hcp at temperature below 77K in high manganese steel of 18Mn as A-T, toughness at low temperature decreases.

In B-T as shown in Fig. 20, total absorbed energy decreases smoothly with decreasing of temperature. Crack initiation energy has a same tendency, as total absorbed energy. As for crack propagation energy, it decreases to the extent of 77K and it does not decrease at 4.2K. Owing to an increasing Mn content and addition of N which is one of elements formed austenite structure in comparison with A-T, product of strain induced martensite is suppressed, therefore, austenite structure is stable and lowering of toughness is improved.

### 3.3 Effect of test temperature on lateral expansion

Lateral expansion in impact test is considered to correspond to plastic deformation capacity. As there exists a proportional relation between lateral expansion and crack opening displacement (COD value), lateral expansion can be considered to be a standard to conclude a toughness of materials through the medium of COD

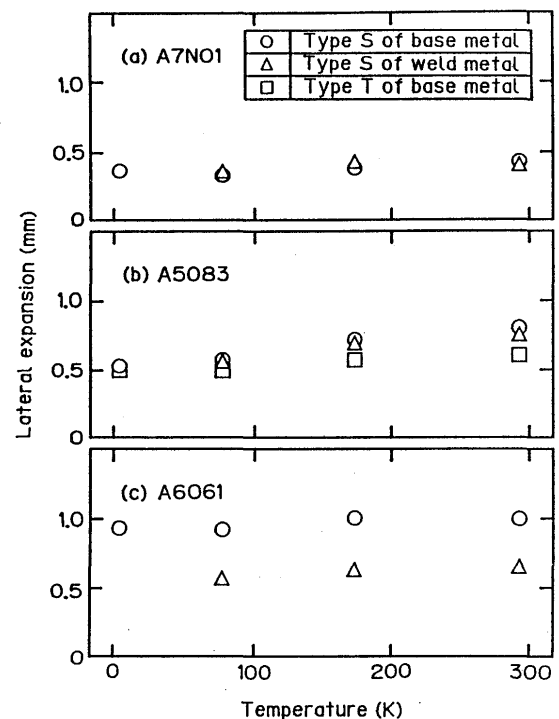


Fig. 22 Change in lateral expansion of Al alloys at various test temperatures.

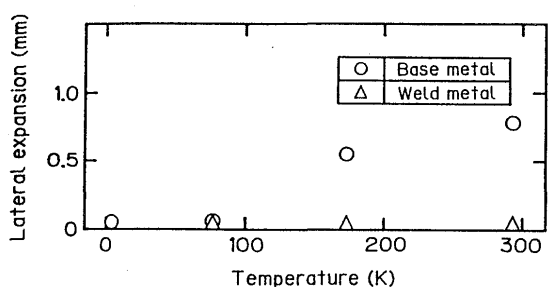


Fig. 23 Change in lateral expansion of JFMS at various test temperatures.

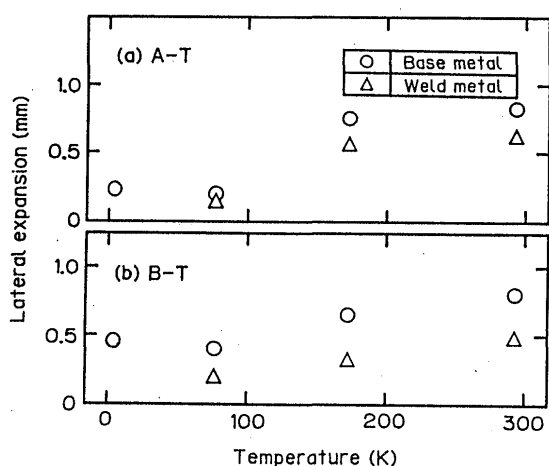


Fig. 24 Change in lateral expansion of high Mn steels at various test temperatures.

value<sup>12)</sup>. Changes in lateral expansion of aluminum alloys, JFMS and high Mn steels at various test temperatures are shown in Fig. 22 ~ 24.

As seen in Fig. 22 lateral expansion of aluminum alloys except A5083 is almost independent of change of temperature. Lateral expansion of A5083 shows a decreasing and smooth tendency with decreasing of temperature. It is different from brittleness due to decreasing of temperature which is generally observed in steels, it depends on hardening caused by an increase of strength.

In Fig. 23, lateral expansion of JFMS base metal decreases rapidly at 77K in particular and it has become brittle. As for weld metal, lateral expansion is close to 0 mm at room temperature, thus, weld metal has become brittle. These results agree with the results of energy.

Figure. 24 shows a good correspondence between the results of lateral expansion and the results of energy of high manganese steels. That is, base metal and weld metal of A-T show a brittle tendency at 77K. On the other hand, lateral expansion of B-T decreases smoothly with decreasing of temperature and there is not very much change of 77K and 4.2 K. It is considered that the difference between A-T and B-T indicates metallurgic

characteristic of stable austenite due to Mn content and addition of N.

#### 4. Conclusion

Main results obtained are as follows.

- (1) In three kinds of aluminum alloys used in experiments, total absorbed energy of A7N01 base and weld metals does not change with decreasing of temperature. A5083 base and weld metals have a decreasing tendency with decreasing of temperature. Although, type T of A5083 shows a unique fracture aspect caused by lamellar flaking, total absorbed energy increases with decreasing of temperature. In base metal of A6061, total absorbed energy increases with decreasing of temperature, though, total absorbed energy of weld metal has a decreasing tendency with decreasing of temperature. Lateral expansion of A7N01 and A6061 is almost independent of change of temperature, decreasing of temperature has a little effect upon toughness. In A5083 except type T, lateral expansion of base and weld metals decreases smoothly with decreasing of temperature, toughness at cryogenic temperature is slightly lower as compared to room temperature.
- (2) Base metal of JFMS shows a brittle at 77K, transition temperature is about 135K. Weld metal has already become brittle at 293K, transition temperature is above room temperature.
- (3) Both base metal and weld metals of A-T decrease abruptly at 77K with decreasing of temperature. It is considered that this decrease is caused by product of strain induced martensite. There is not much difference base metal and weld metal, thus, it is independent of welding.
- (4) In B-T, when temperature drops, load increases and total absorbed energy decreases. But values of load and energy are higher as compared to A-T. It is considered that increasing Mn content and addition of N can make austenite structure stable and retard a decreasing of toughness at cryogenic temperature.

#### References

- 1) Society of Atomic Energy Engineering; Present State and Problem of Designing and Research Development of Nuclear Fusion Reactor (1983) (in Japanese)
- 2) Energy Special Research (Nuclear Fusion) Group of Heavy Irradiation; "Progress of Heavy Irradiation Research", Total Report, (1986), 183-203 (in Japanese)
- 3) T. Matsuoka, et al; J. Iron & Steel Inst., Vol.67, No.2, (1981), A89-A92 (in Japanese)
- 4) Y. Ootani, et al; Sumitomo Metals, Vol.38, No.1, (1986), 1-9 (in Japanese)
- 5) T. Kajino and T. Kobayashi; J. Iron & Steel Inst., Vol.66,

- (1980), 159-160 (in Japanese)
- 6) T. Ogata, et al; J. Iron & Steel, Vol.69, No.6, (1983), 641-646 (in Japanese)
  - 7) K. Higashi, et al; J. of Japan Inst. of Light Metals, Vol.32, No.1, (1982), 8-13 (in Japanese)
  - 8) K. Asano and A. Fujiwara; J. of Japan Inst. of Light Metals, Vol.26, No.1, (1976), 27-34 (in Japanese)
  - 9) T. Kobayashi and K. Takai; J. of Japan Inst. of Light Metals, Vol.22, No.9, (1982), 541-554 (in Japanese)
  - 10) S. Kaga, et al; Quarterly J. of Japan Welding Society, Vol.7, No.1, (1989), 27-33 (in Japanese)
  - 11) J. Namekata; J. of JFMS, Vol.18, No.1, (1983), 18-39 (in Japanese)
  - 12) T. Takaai and A. Daitoh; J. of Japan Inst. of Light Metals, Vol.34, No.10, (1984), 557-561 (in Japanese)